Urban Climate 66 (2026) 102828

Contents lists available at ScienceDirect

Urban Climate

journal homepage: www.elsevier.com/locate/uclim

Quantifying mobility-based seasonal individual heat exposure and the NEAP using multi-source spatiotemporal data

Yan Zhang [a,b], Mei-Po Kwan [a,b,*], Zhijie Zhang [c]

[a] Department of Geography and Resource Management, Wong Foo Yuan Building, The Chinese University of Hong Kong, Hong Kong SAR, China
[b] Institute of Space and Earth Information Science, Fok Ying Tung Remote Sensing Science Building, The Chinese University of Hong Kong, Hong Kong SAR, China
[c] School of Geographic Sciences, Hebei Normal University, Shijiazhuang, Hebei, China

ARTICLE INFO

Keywords:
Heat exposure
Human mobility
Exposure disparity
Socioeconomic status
Neap

ABSTRACT

Under the dual drivers of global climate change and urbanization, heat waves have become one of the severe challenges to urban residents' health. This study investigates the neighborhood effect averaging problem (NEAP) across different socioeconomic status groups and seasons by integrating mobile phone signaling data, high-resolution land surface temperature remote sensing data, and cumulative exposure modeling. Using Hangzhou as the study area, we compared residents' mobility-based exposure (MBE) and residence-based exposure (RBE) based on mobility trajectory data from 5,747 (summer) and 6,167 (winter) residents. The study reveals: (1) Approximately 65% of residents experienced heat exposure mean reversion at both seasons, strongly validating the existence of the NEAP in heat exposure; (2) Human mobility behavior tends to reduce heat exposure levels in summer (MBE: 39.75°C, RBE: 39.85°C) while increasing exposure levels in winter (MBE: 13.89°C, RBE: 13.79°C); (3) Different socioeconomic status groups exhibited significantly different exposure patterns, with low socioeconomic status residents showing more pronounced NEAP in summer and the opposite in winter, while low SES groups faced higher heat exposure risks during summer. This study overcomes the limitations of traditional survey methods' insufficient spatial coverage and high costs, revealing the systematic regulatory effect of human mobility behavior on heat exposure. It also provides case evidence for developing social equity and urban climate adaptation policies.

1. Introduction

Under the dual drivers of global climate change and rapid urbanization, heat waves have emerged as one of the most severe urban public health challenges of the 21st century. The Sixth Assessment Report of the Intergovernmental Panel on Climate Change (IPCC) indicates that the frequency of extreme heat events globally showed an increasing trend from 1980 to 2020, with urban areas experiencing higher proportions of population exposure to extreme heat risks compared to rural areas due to the Urban Heat Island (UHI) effect (Ma et al., 2023; Huang et al., 2024). Statistics show that over the past two decades, the urban population affected by extreme heat has increased by 115 million, while the area impacted by excessive urban heat exposure has expanded by 78.91% (Liu

* Corresponding author at: Institute of Space and Earth Information Science, Fok Ying Tung Remote Sensing Science Building, The Chinese University of Hong Kong, Hong Kong SAR, China.

E-mail addresses: yanzhang@cuhk.edu.hk, sggzhang@whu.edu.cn (Y. Zhang), mpkwan@cuhk.edu.hk (M.-P. Kwan), 20200813054@sjzc.edu.cn (Z. Zhang).

https://doi.org/10.1016/j.uclim.2026.102828
Received 29 May 2025; Received in revised form 25 November 2025; Accepted 11 February 2026
Available online 21 February 2026
2212-0955/

et al., 2024; Wang et al., 2024a). Substantial epidemiological evidence indicates significant correlations between heat exposure and cardiovascular diseases, cognitive dysfunction, and all-cause mortality (Münzel et al., 2023). Against this backdrop, accurately assessing dynamic heat exposure at the individual level has become a crucial scientific question for identifying vulnerable populations and optimizing urban climate adaptation policies.

Traditional heat exposure assessment methods primarily rely on meteorological station observations or static residence-based exposure (RBE) models, assuming individuals are static and remain within single geographic units (residences or workplaces). However, the spatiotemporal mobility of human activities has thoroughly disrupted this simplified framework. Empirical studies indicate that individual daily activity trajectories can lead to significant disparities between actual heat exposure (mobility-based exposure, MBE) and RBE assessment results (daily activities may amplify or diminish actual exposure levels), manifesting the neighborhood effect averaging problem (NEAP) (Kwan, 2018). The NEAP refers to the problem that individual mobility-based exposures to environmental factors tend toward the mean level of the participants or population of a study area when compared to their residence-based exposures. Note that a typical human mobility pattern for a working adult involves 8 h at home, 8 h at work, and 8 h in leisure activities. For instance, Yasumoto et al. (2019) found in Dhaka that commuters' daytime peak heat exposure was higher than at their residences, indicating that RBE-based measures underestimated people's heat exposure levels. Similarly, a comparative study in San Diego, USA, reached comparable conclusions, with MBE-based average maximum surface temperature at 40.3 °C compared to RBE-based average maximum surface temperature at 35.8 °C (Garber et al., 2024). These findings highlight how traditional methods that ignore human mobility dynamics may exacerbate biases in heat exposure risk assessment, a critical issue emphasized in recent scholarly discussions on the necessity of mobility-based assessments (Zhang and Kwan, 2025).

Fig. 1 illustrates how MBE and RBE are evaluated, showing one person's daily movement trajectory. Compared to RBE calculation, MBE takes environmental exposure along people's travel routes and at their visited locations into account. This figure effectively demonstrates how individuals interact with urban spaces throughout the day, revealing a typical pattern of human daily movement and activity space during a workday.

Recent breakthroughs in spatiotemporal big data technology have opened new pathways for dynamic heat exposure assessment in urban areas. Methods integrating GPS real-time tracking, wearable sensors, and multi-source remote sensing data can capture individual activity trajectories and heat exposure information at a minute-level resolution (Liu et al., 2023), more accurately recording exposure levels, locations, and durations in daily life. These citizen science-based mobile exposure sensing studies have achieved significant breakthroughs (Cai and Kwan, 2024; Song et al., 2025). However, while these advanced mobile methods provide detailed records, cost constraints often limit coverage to small populations. As a result, there is still a lack of large-scale mobility-based individual heat exposure assessments (Wang et al., 2018; Wang et al., 2024b). Furthermore, although Kumakura et al. (2024) calculated Tokyo residents' daily heat exposure dynamics using mobile phone signaling data, they considered neither cumulative heat exposure effects nor seasonal variations. Additionally, due to privacy considerations and restrictions, compared to citizen science methods, spatiotemporal big data approaches often lack individuals' information (e.g., sociodemographic attributes) and crucial residential location data for RBE calculations, limiting their application in human mobility exposure studies (Kwan, 2016).

Addressing these issues, this study proposes a human heat exposure assessment framework integrating mobile phone signaling data, high-resolution land surface temperature (LST) retrieval, and exposure accumulation models. We used Hangzhou, China, a high-density Asian city, as the study area. The research's innovations are threefold. First, it employs mobile phone signaling data for dynamic exposure trajectory modeling, transcending the limitations of traditional static exposure points by introducing time-weighted cumulative exposure calculations to quantify individual RBE and MBE (Yin et al., 2021). Second, it uses clustering algorithms to identify residential addresses while incorporating housing price data to define people's socioeconomic status (SES). Finally, it considers seasonal impacts on heat exposure, examining the significance of the NEAP's effects in both winter and summer.

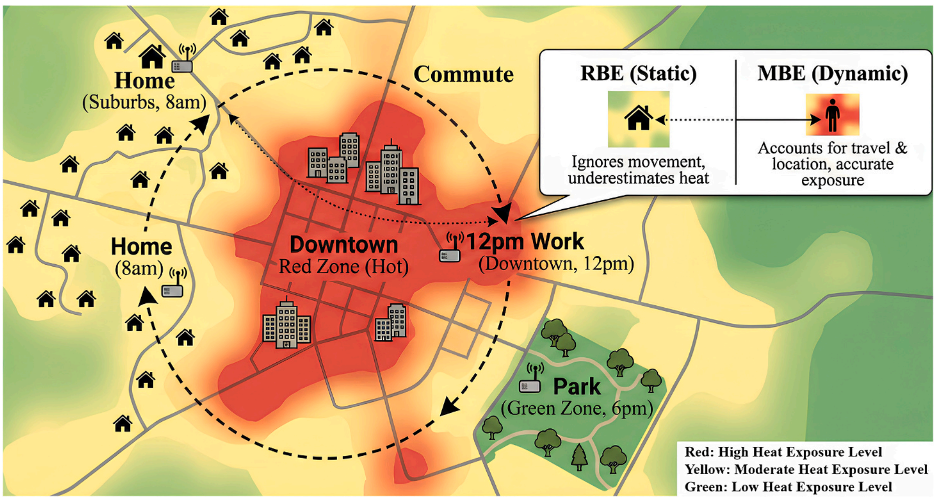

Fig. 1. Visualization of an individual's daily movement trajectory and activity locations across an urban area.

2. Related work

Given the inherent limitations of assessing people's environmental exposure levels solely based on their residential or workplace locations, incorporating human mobility into exposure assessment has become increasingly important. For instance, while Chen et al.'s (2022) study considered population distribution patterns, it could only obtain the spatially weighted distribution state of residents, with their WorldPop data lacking temporal dynamics. Subsequently, Zhang et al. (2024a, 2024b) evaluated urban population heat exposure status at different times using multi-temporal land surface temperature (LST) data, but their analysis was limited to residential population information. Moreover, significant disparities in exposure levels exist among different population groups, with older adults often facing higher heat exposure levels (Falchetta et al., 2024) and lower mobility (Malekzadeh et al., 2024). Heat exposure is also strongly related to socioeconomic status (Nilforoshan et al., 2023). Given these limitations, comprehensively capturing individual mobility using GPS trajectories and perceived exposure values becomes crucial.

In recent years, researchers in Beijing and Hong Kong have developed and implemented advanced mobile methods for evaluating individuals' mobility-based exposures to various environmental factors, including green spaces, light at nights, air pollution and noise (Liu et al., 2025a, 2025b; Wang et al., 2025b). Their projects involved hundreds of participants and employed mobile sensors for data collection. The results of these studies demonstrated that incorporating human mobility could improve the accuracy of exposure assessment compared to traditional static evaluations (Liu et al., 2025a, 2025b). Similar results were also observed in European studies, which expand our knowledge boundary about environmental exposure (Wei et al., 2024; Wei et al., 2025). This mobility-based exposure measurement approach is more accurate and refined than traditional residence-based exposure methods, as people's daily movement and activities may amplify or diminish their actual exposure levels due to neighborhood effect averaging.

Previous NEAP studies typically focus on individual cities. Given the large urban scale, these studies required substantial resources (recruiting participants and purchasing sensing equipment) to achieve comprehensive urban coverage. With the advancement of communication infrastructure, spatiotemporal big data methods have emerged as an (Zhang et al., 2026) alternative solution. These include mobile phone signaling data (Wang et al., 2024b; Wang et al., 2025a), social media data (Hu et al., 2021; Li et al., 2021), and APP usage data (Schläpfer et al., 2021). However, these methods typically only capture individuals' trajectories and require high-resolution environmental sensing data to obtain their actual exposure levels. High spatiotemporal resolution remote sensing data (including data on air pollution, the normalized difference vegetation index, and land surface temperature) (Wei et al., 2021) and street view imagery (Sabedotti et al., 2023; Chen et al., 2024; Zhang et al., 2024a, 2024b; Zhang et al., 2025) are commonly used to assess people's exposure levels.

Nevertheless, when comparing RBE and MBE values, two key challenges remain: identifying household address information and

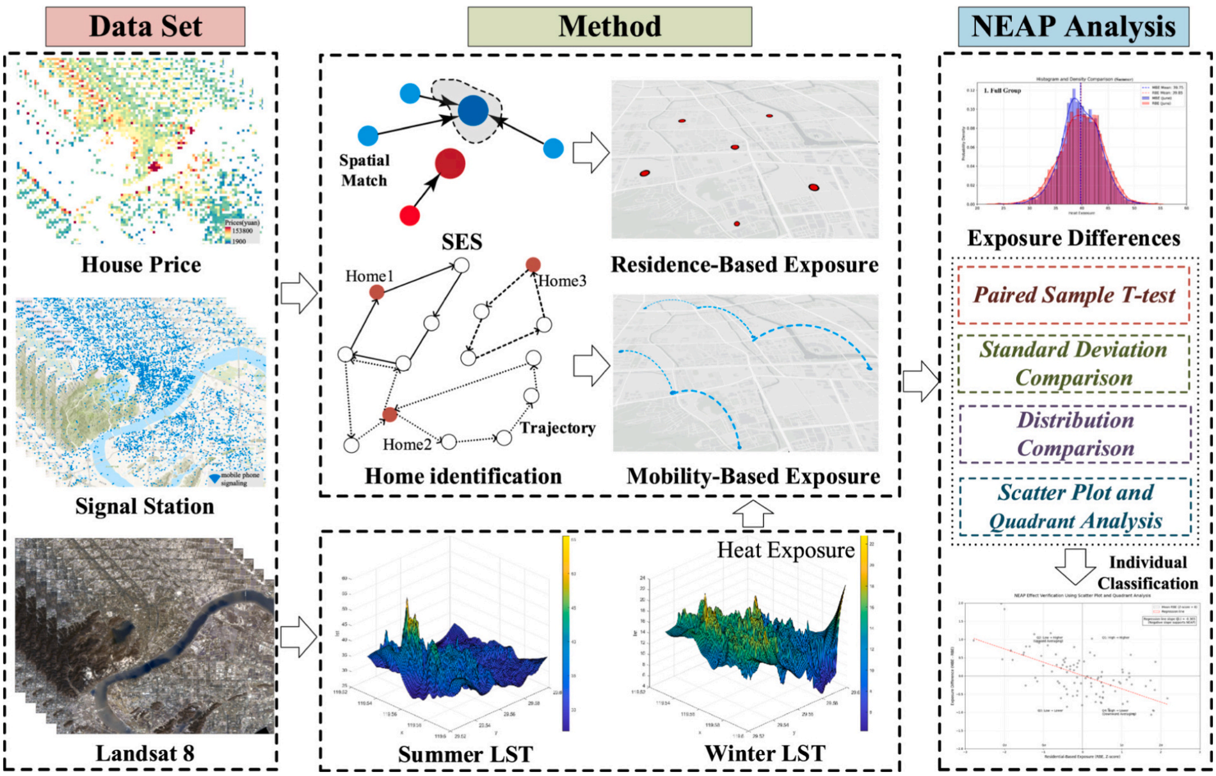

Fig. 2. The flowchart of this framework: including the collection and processing of multi-source spatiotemporal big data for calculating individual seasonal heat exposure.

extracting population features from spatiotemporal trajectory big data. Furthermore, using heat exposure as an example, summer and winter heat exposures have differing impacts on residents' health, and mobility patterns can also vary seasonally, while discussions on the influence of seasonality and varying socioeconomic status on the NEAP remain insufficient (Zhang et al., 2024a).

3. Data and methods

To summarize the entire methodological procedure, Fig. 2 presents a comprehensive flowchart of the research framework. It illustrates the complete process, from the collection and processing of multi-source spatiotemporal big data, to the calculation of individual seasonal heat exposure (RBE and MBE) for different SES groups, and finally, the application of four statistical methods to examine the intensity of the NEAP.

3.1. Research area and research data

This study focuses on Hangzhou, the capital and largest city of Zhejiang Province, China (Fig. 3). The mobility trajectory data was obtained from a telecommunications operator covering the period from June 1st to June 30th, 2018. The dataset comprises 150,513,330 records, each containing an anonymized user ID, timestamp of base station connection, and the geographical coordinates of the cell tower base station. The study area is well-covered by 16,186 cell tower base stations, with an average nearest-neighbor distance of 325.07 m, indicating dense spatial coverage that minimizes potential bias from point-based LST measurements. The dataset includes 394,081 anonymized users. While the operator's exact market share is confidential, it is one of China's three largest providers, suggesting the sample is substantial and broadly representative of the population's geographic distribution in Hangzhou.

As NEAP analysis typically focuses on individual cities, we specifically filtered and extracted data from Hangzhou City. Our study area has a high-density network of base stations. For each resident, we tracked which base station they were connected to at different times. We then used the heat environmental conditions around each connected base station to estimate the user's exposure at that specific time. The duration of exposure was calculated based on how long users remained connected to each base station.

To assess residents' socioeconomic status, we incorporated housing price data from Anjuke (one of China's largest real estate websites), collecting 9797 community housing price records (Wang et al., 2018). This dataset includes geographical coordinates of residential communities, average house price, floor area ratios, and other relevant metrics to define residents' socioeconomic status (SES) (Wang et al., 2018).

For accurate measurement of residents' heat exposure, we utilized Landsat 8 satellite imagery data as a proxy indicator, which has an overpass time of approximately 10:30 AM local time. The satellite imagery corresponds to the same year as the mobile phone signaling data. The Land Surface Temperature (LST) dataset was derived from Landsat satellite imagery with 30 m spatial resolution and a 16-day temporal resolution (satellite revisit period). To account for cloud cover impacts on LST data integrity, we calculated average temperatures using satellite data from May 15th to July 15th for summer exposure and from November 15th of the previous year to January 15th of the current year for winter exposure. While LST typically exceeds air temperature measurements, particularly during direct sunlight conditions, it remains a relatively objective and reliable heat exposure indicator that has been widely applied in numerous heat exposure studies (Yuan et al., 2022). It is important to note that LST represents the outdoor surface temperature. As the mobile phone data does not distinguish between indoor and outdoor locations, our calculation of "heat exposure" refers to the ambient outdoor LST at a person's location, which serves as a proxy for potential exposure. This approach does not account for micro-environments or protective behaviors (e.g., being inside an air-conditioned building).

Our study utilized the Google Earth Engine (GEE) platform, accessing the public Landsat 8 Collection 2 Level 2 (LANDSAT/LC08/C02/T1_L2) data product. This dataset features improvements in cloud masking, radiometric correction, geometric correction, and surface reflectance products, which significantly improve LST data quality and accuracy. We selected Band 10 (STB10) for LST extraction, when applied with appropriate scaling factors and conversion formulas, directly yields LST values (resident heat exposure levels).

We identified approximately 46,371 residential locations and excluded residents with significant missing heat exposure data (as excessive missing data could affect MBE accuracy). Then, we filtered for users residing within Hangzhou city limits.

This study utilizes mobility data from a single month (June) for both summer and winter analyses. This approach rests on the assumption that individuals' core spatial mobility patterns (e.g., commute routes) are largely consisten. The dataset includest across seasons, allowing us to isolate the effect of seasonal LST variations on heat exposure. The analysis aggregates data over the entire month, thus capturing an average mobility pattern that includes both weekday and weekend activities, rather than treating them separately. Regarding data privacy and accuracy, the mobile phone signaling data was fully anonymized by the telecommunications operator before acquisition, meaning no personal attributes such as name or age were included. Consequently, "household address information" in this study refers to the geographical coordinates of residential locations estimated using a clustering algorithm, with accuracy at the cell tower level, representing an approximate residential area rather than a precise address. Similarly, the "population features" extracted are limited to the socioeconomic status, which was inferred by spatially joining the estimated residential location with community-level housing price data. The temporal resolution of the mobility data is based on the timestamp of the user's connection to a base station. The assumption of applying a single month's mobility pattern to both seasons is a key limitation of this study, which is further addressed in the Discussion section.

The conceptual foundation of MBE is rooted in the NEAP framework (Kwan, 2018), which posits that individual exposures to environmental factors, such as heat, tend toward the population mean when mobility is considered, compared to static residence-based measures. This averaging effect arises because daily activities expose individuals to a broader range of environments, potentially

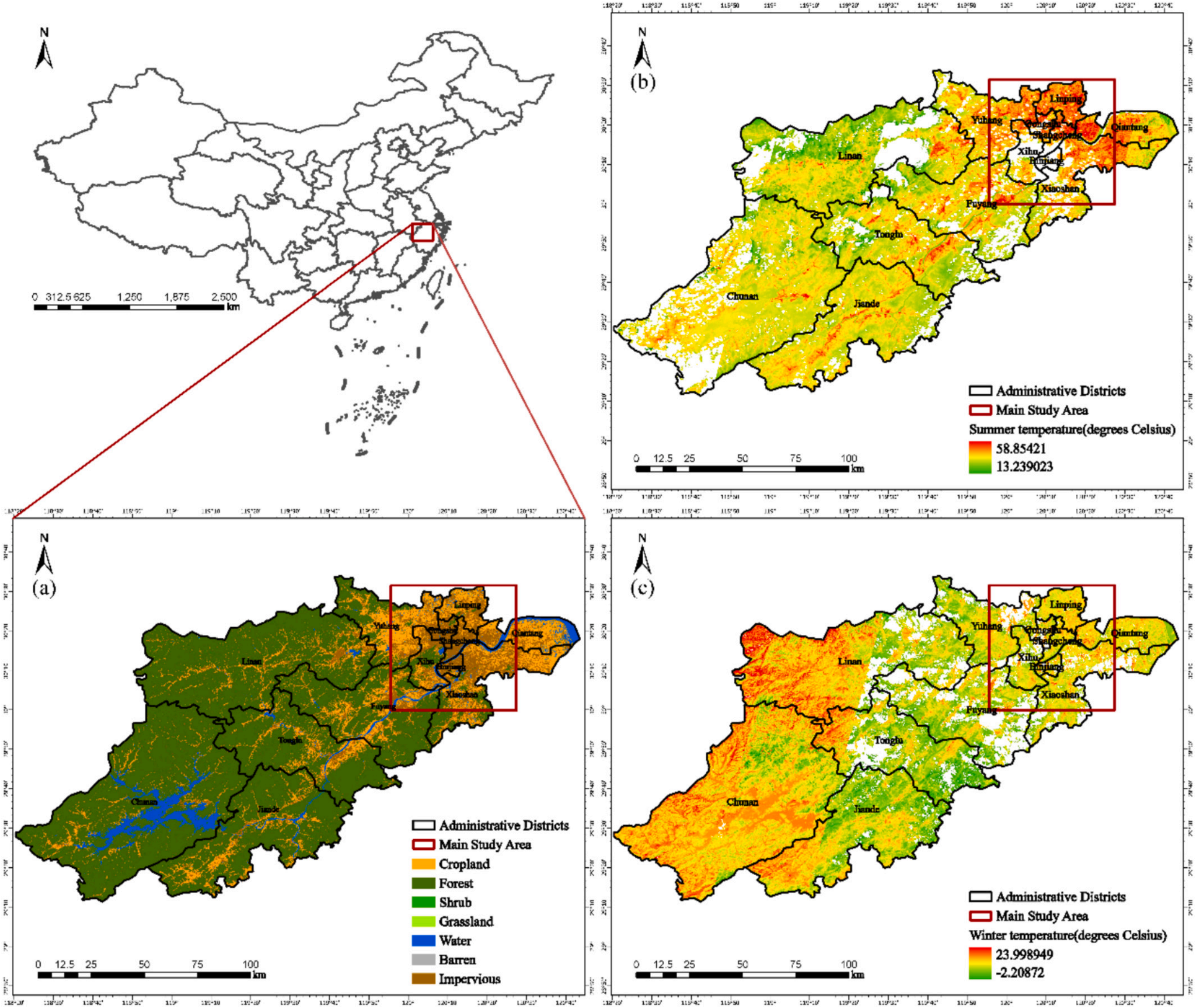

Fig. 3. The study area and Land Surface Temperature exposure data.

mitigating or amplifying residence-specific risks.

3.2. Spatiotemporal data fusion and exposure calculation

To quantify individual heat exposure, we fused the human mobility trajectories with the high-resolution Land Surface Temperature (LST) data. The study area is well-covered by 16,186 cell tower base stations, with a high density in the urban core, ensuring comprehensive tracking of user movements. The coverage of a single base station varies from approximately 300 m in dense urban areas to a few kilometers in suburban regions. For each user, their trajectory was represented as a sequence of timestamped points, where each point corresponds to the location of the connected cell tower base station. The LST value at each point was extracted from the seasonal LST raster maps (Fig. 3). The user's exposure at any given time was assumed to be the LST value of the grid cell containing the base station they were connected to.

3.2.1. Residence-based exposure(RBE)

RBE is defined as the average Land Surface Temperature (LST) of the grid cell where the identified home is located.

$$RBE_i = \left(x_{home,i}, y_{home,i}\right)$$

where $\left(x_{home,i}, y_{home,i}\right)$ are the coordinates of the identified home location for individual *i*.

3.2.2. Mobility-based exposure(MBE)

MBE is defined as the time-weighted average of LST at all locations (represented by cell tower locations) a user visits during the observation period. The formula is:

$$MBE_i = \frac{\overline{\sum_{j=1}^{N} \left(LST(x_i, y_i) \times t_j\right)}}{\sum_{j=1}^{N} t_j}$$

where for individual *i*, *N* is the total number of recorded locations (base station connections), $\left(x_i, y_i\right)$ are the coordinates of the *j*-th location, $LST\left(x_i, y_i\right)$ is the LST at that location, and t_i is the duration of the stay at that location.

It should be noted that MBE represents a relative exposure measure that incorporates individual mobility patterns rather than absolute heat exposure values. While LST provides a spatially consistent thermal proxy that captures heterogeneity across different urban environments, the primary contribution of MBE lies in weighting these relative thermal conditions by actual time allocation based on individual movement trajectories. This approach provides a more realistic assessment of an individual's cumulative heat exposure throughout their daily activities, including both residential and non-residential time allocation, which is essential for capturing the complete exposure profile as established in mobility-based exposure methodology (Wei et al., 2025).

In addition, the integration of daily mobility data (dynamic trajectories from mobile signaling with seasonal average LST (fixed at 10:30 AM overpass time) serves as a proxy for individual heat exposure at the seasonal scale. While LST captures typical outdoor thermal conditions, mobility data weights exposure by time spent at each location. This relationship allows us to interpret MBE as a measure of cumulative potential exposure, though it does not account for intra-day variations or indoor mitigations (e.g., air conditioning). This conceptual approach highlights how mobility regulates exposure toward the mean, as evidenced by the NEAP analysis.

3.3. Methods for examining the NEAP

The NEAP refers to the phenomenon where individuals' mobility-based environmental exposure tends toward the mean level of participants or population in the study area compared to residence-based exposure (Kim and Kwan, 2021a; Cai and Kwan, 2024). This concept involves two key components: mobility-based exposure (MBE) and residence-based exposure (RBE), whose difference reflects whether people's daily mobility amplifies or diminishes their exposure experienced in their residential communities, while traditional exposure calculations centered on residence or workplace may overestimate or underestimate residents' actual exposure levels. Previous NEAP-related research has shown that four methods can be employed to test for the presence of NEAP effects, including paired sample *t*-tests, standard deviation comparison, frequency distribution comparison, and scatter plot analysis (Kim and Kwan, 2021a; J. Huang and Kwan, 2022; Cai and Kwan, 2024).

3.3.1. Paired sample t-test

The paired sample t-test is used to compare whether there are significant differences between RBE and MBE measures for the same group of subjects. Paired sample t-tests were used because MBE and RBE represent paired observations from the same individuals, with the null hypothesis being no difference between mobility-based and residence-based exposure. The t-statistics are calculated as follows:

$$t = \frac{\overline{d}}{s_d/\sqrt{n}}$$

where: $\overline{d}$ is the mean of differences, $\overline{d} = \frac{1}{n}\sum_{i=1}^{n}(RBE_i - MBE_i)$, s_d is the standard deviation of differences, and n is the size of the sample. The t-test uses p-value to indicate the significance level of the difference, with the p-value calculated through the cumulative distribution function of the t-distribution:

$$p = 2 \times P(T > |t|)$$

If $p < 0.05$, it indicates a statistically significant difference between RBE and MBE. The sign of the t-statistic indicates the direction of the difference (positive values indicate that RBE is greater than MBE, negative values indicate that MBE is greater than RBE). A significant difference supports the existence of the NEAP, suggesting that people's mobility behavior indeed changes their heat exposure levels when compared to their residence-based exposures.

3.3.2. Standard deviation comparison

The comparison of standard deviations between RBE and MBE examines whether mobility behavior reduces the variability in heat exposure. The NEAP predicts that human mobility behavior leads to a more concentrated distribution of heat exposure. Therefore, the standard deviation of MBE should be smaller than that of RBE when there is neighborhood effect averaging. The formulas for standard deviation comparison are as follows:

RBE Standard Deviation:

$$\sigma_{RBE} = \sqrt{\frac{1}{n}\sum_{i=1}^{n}(RBE_i - \overline{RBE})^2}$$

MBE Standard Deviation:

$$\sigma_{MBE} = \sqrt{\frac{1}{n}\sum_{i=1}^{n}(MBE_i - \overline{MBE})^2}$$

Standard Deviation Reduction Percentage:

$$std_{reduction} = \frac{\sigma_{RBE} - \sigma_{MBE}}{\sigma_{RBE}} \times 100\%$$

When the standard deviation of MBE is smaller than that of RBE, it indicates that mobility behavior reduces exposure variability, aligning with NEAP predictions. The standard deviation reduction percentage ($std_{reduction}$) measures the extent of this reduction, with a higher reduction percentage indicating a stronger NEAP effect, reflecting that mobility behavior has a stronger concentrating effect on the distribution of heat exposure. The higher the standard deviation reduction percentage, the stronger the NEAP effect.

3.3.3. Frequency distribution comparison

By comparing the frequency distribution characteristics of RBE and MBE (interquartile range IQR and proportion of near-mean samples, defined as samples within mean $\pm$ 0.5 standard deviation), we further examine whether the NEAP effect leads to more concentrated heat exposure distribution. The NEAP effect predicts that the distribution of MBE will be more concentrated around the mean than the distribution of RBE. The formulas for interquartile range calculation are:

$$IQR_{RBE} = Q3_{RBE} - Q1_{RBE}$$

$$IQR_{MBE} = Q3_{MBE} - Q1_{MBE}$$

where $Q1$ and $Q3$ are the 25th and 75th percentiles respectively:

$$Q1_{RBE} = Percentile_{25}(RBE) \; Q3_{RBE} = Percentile_{75}(RBE)$$

IQR reduction percentage:

$$iqr_{reduction} = \frac{IQR_{RBE} - IQR_{MBE}}{IQR_{RBE}} \times 100\%$$

Near-mean sample proportion:

$$RBE_{near\_mean} = \frac{|i : \overline{RBE} - 0.5\sigma_{RBE} \leq RBE_i \leq \overline{RBE} + 0.5\sigma_{RBE}|}{n} \times 100\%$$

Near-mean sample increase is the difference between MBE_{near_mean} and RBE_{near_mean}. A reduction in interquartile range (IQR) indicates that MBE distribution is more concentrated than RBE, while an increase in the near-mean sample proportion indicates that more individuals are concentrated around the mean. Both metrics are used to test the equalizing characteristic of the NEAP, examining whether human mobility behavior makes the extreme heat exposure density distribution curve smoother.

3.3.4. Scatter plot and quadrant analysis

This method examines the relationship between RBE and MBE through regression analysis. The NEAP predicts that individuals with high RBE values will have lower MBE values, while those with low RBE values will have higher MBE values, resulting in a regression slope less than 1 between RBE and MBE-RBE differences.

RBE standardization:

$$RBE_{z_i} = \frac{RBE_i - \overline{RBE}}{\sigma_{RBE}}$$

Difference calculation:

$$diff_i = MBE_i - RBE_i$$

Linear regression:

$$diff_i = \beta_0 + \beta_1 \times RBE_{z_i} + \epsilon_i$$

where β_1 is the slope, calculated using least squares method:

$$\beta_1 = \frac{\sum_{i=1}^{n} \left(RBE_{z_i} - \overline{RBE_z}\right)\left(diff_i - \overline{diff}\right)}{\sum_{i=1}^{n} \left(RBE_{z_i} - \overline{RBE_z}\right)^2}$$

Quadrant proportion calculation:

$$q1 = \frac{\left|i : RBE_{z_i} > 0 \text{ and } diff_i > 0\right|}{n} \times 100\%$$

$$q2 = \frac{\left|i : RBE_{z_i} < 0 \text{ and } diff_i > 0\right|}{n} \times 100\%$$

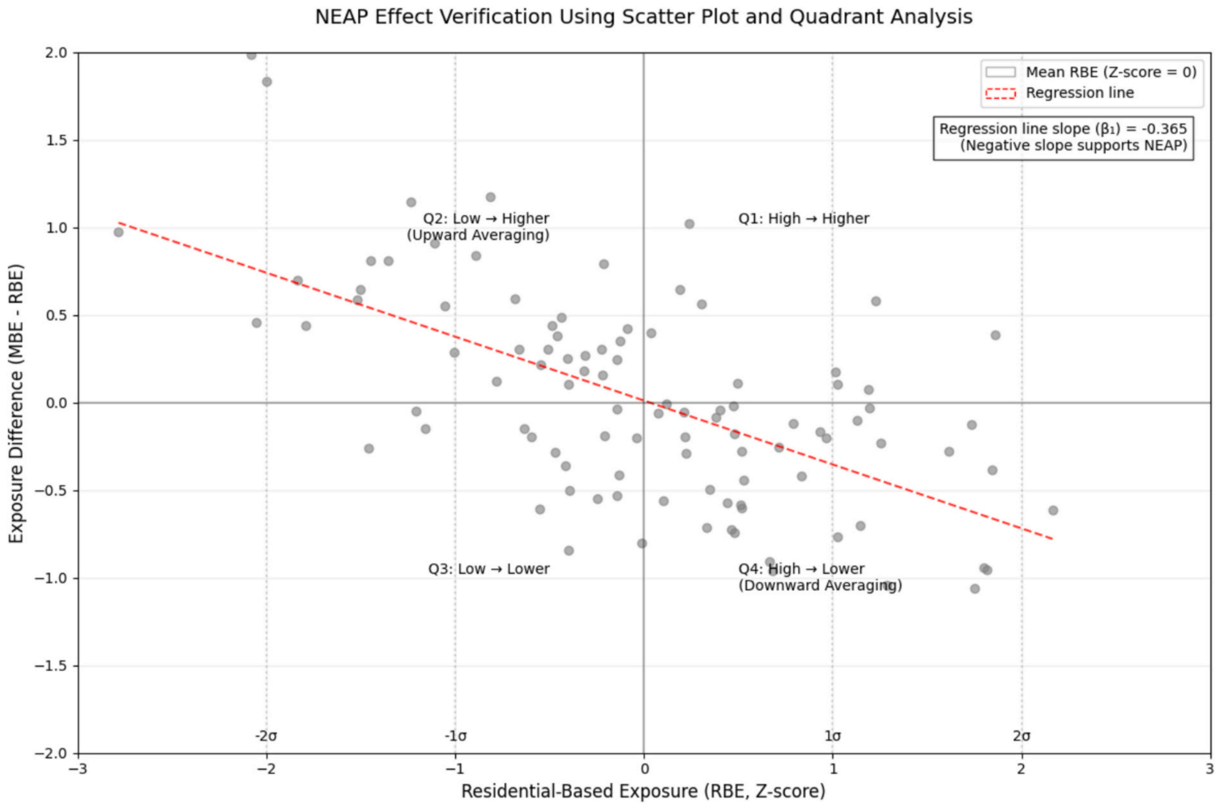

Fig. 4. The illustration of verification of the NEAP effect using quadrant analysis and scatter plot. The x-axis shows the standardized residence-based exposure (RBE, z-score), while the y-axis represents the exposure difference between mobility-based and residence-based exposure (MBE-RBE). The negative slope (β_1) supports the NEAP hypothesis. The four quadrants represent different NEAP patterns: Upward Polarization (Q1), Upward Averaging (Q2), Downward Polarization (Q3), and Downward Averaging (Q4), with Q2 and Q4 supporting the NEAP hypothesis.

$$q3 = \frac{|i : RBE_{z_i} < 0 \text{ and } diff_i < 0|}{n} \times 100\%$$

$$q4 = \frac{|i : RBE_{z_i} > 0 \text{ and } diff_i < 0|}{n} \times 100\%$$

NEAP evidence proportion:

$$NEAP_{evidence} = q2 + q4$$

A negative slope ($\beta_1 < 0$) indicates that as RBE increases, the MBE-RBE difference decreases, supporting the NEAP. The core hypothesis of the NEAP is that exposure differences between residential areas tend to average out when considering people's mobility. In quadrant analysis, the second quadrant (low values rising) and fourth quadrant (high values falling) represent individuals conforming to the NEAP. The first quadrant (high values unexpectedly rising) and third quadrant (low values unexpectedly falling) represent individuals contrary to the NEAP. The higher the proportion of individuals conforming to the NEAP, the more significant the NEAP effect. As shown in Fig. 4, NEAP patterns can be classified into four categories based on different quadrants: Downward Averaging (Q4, a typical NEAP case) and Upward Averaging (Q2, a typical NEAP case), representing the tendency toward exposure averaging, along with Downward Polarization (Q3, an extreme NEAP case) and Upward Polarization (Q1, an extreme NEAP case), indicating deviation from the averaging effect. The strength of the NEAP effect can be quantified either by the proportion of individuals falling into Q2 and Q4, or by the magnitude of the regression slope (β_1).

When the slope is close to 1 (e.g., 0.95–1.05), RBE and MBE are almost proportional, indicating that overall exposure is like residential exposure, regardless of residential heat exposure, suggesting an insignificant NEAP effect. When the slope is significantly less than 1 (e.g., 0.7 or lower), it indicates that individuals with high RBE values have lower MBE values (relative to the ideal case y = x), and individuals with low RBE values have higher MBE values, which is the core characteristic of the NEAP effect's equalizing effect. The smaller the slope, the more significant the NEAP effect.

In this scatter plot (Fig. 4), the X-axis represents the standardized RBE values (Z-scores) ($\frac{RBE - \overline{RBE}}{\sigma_{RBE}}$), and the Y-axis represents the difference between MBE and RBE (MBE - RBE). We can classify each observation point into one of four quadrants (Q1-Q4), with each quadrant representing different patterns of change from RBE to MBE. The advantage of using Z-scores is that they convert data of different scales to the same standardized scale. Instead of focusing on absolute exposure levels, it focuses on high or low levels relative to the population mean, facilitating comparisons across different regions, time periods, or studies.

The first quadrant (Q1: High RBE values unexpectedly increasing) is characterized by RBE > mean value and MBE > RBE. Residents in this area typically live in high-exposure areas, and when their mobility is considered, their exposure levels further increase (meeting conditions $rbe_z > 0$ & $diff > 0$). In the second quadrant (Q2: Low RBE values further increasing), the most notable characteristic is RBE < mean value and MBE > RBE. This means residents in this quadrant typically live in low-exposure areas, but when their mobility is considered, their exposure levels increase ($rbe_z < 0$ & $diff > 0$).

The third quadrant (Q3: Low RBE values unexpectedly decreasing) is characterized by RBE below average and MBE < RBE, indicating that residents in low-exposure areas experience further reduced exposure levels when considering their daily mobility, with conditions requiring both standardized RBE values less than zero ($rbe_z < 0$) and negative exposure difference values ($diff < 0$). The fourth quadrant (Q4: High RBE values further decreasing) shows RBE above average but MBE < RBE, reflecting that residents in high-exposure areas experience decreased actual exposure levels due to mobility, requiring conditions of standardized RBE values greater than zero ($rbe_z > 0$) and negative exposure difference values ($diff < 0$).

These four methods were used in past studies to examine the NEAP intensity from different angles. Together, the comprehensive analysis can more thoroughly evaluate the existence and strength of the NEAP effect. When multiple methods support the NEAP effect, the conclusions become more reliable.

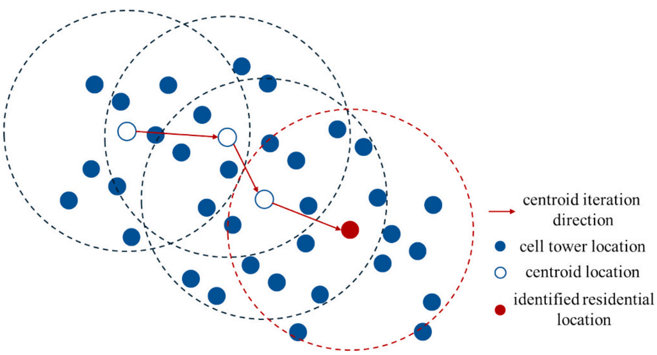

Fig. 5. Residential location identification using time-weighted K-means clustering. The algorithm iteratively determines the optimal centroid position (white circles) based on nighttime cell tower locations (blue dots), ultimately identifying the residential location (red dot). (For interpretation of the references to colour in this figure legend, the reader is referred to the web version of this article.)

3.4. Identify home locations from mobile phone signaling data

To identify home locations from mobile phone signaling data, we used a time-weighted K-means clustering approach. The method consists of three main steps: temporal filtering, time-weight assignment, and weighted clustering. The time-weighted K-means clustering process for residential location identification is presented in Fig. 5. Blue dots represent cell tower locations where mobile phone signals were detected during nighttime hours (00:00–06:00). White circles show the intermediate centroid positions during the iteration process, with dashed circles indicating their respective clustering regions. The red arrow indicates the direction of centroid iteration, and the final red dot marks the identified residential location. The convergence of the algorithm is achieved through multiple iterations that minimize the weighted distance between the centroid and cell tower locations.

To be specific, we first extract nighttime stay points between 00:00 and 06:00, applying a minimum duration threshold of 2 h to filter out transient locations:

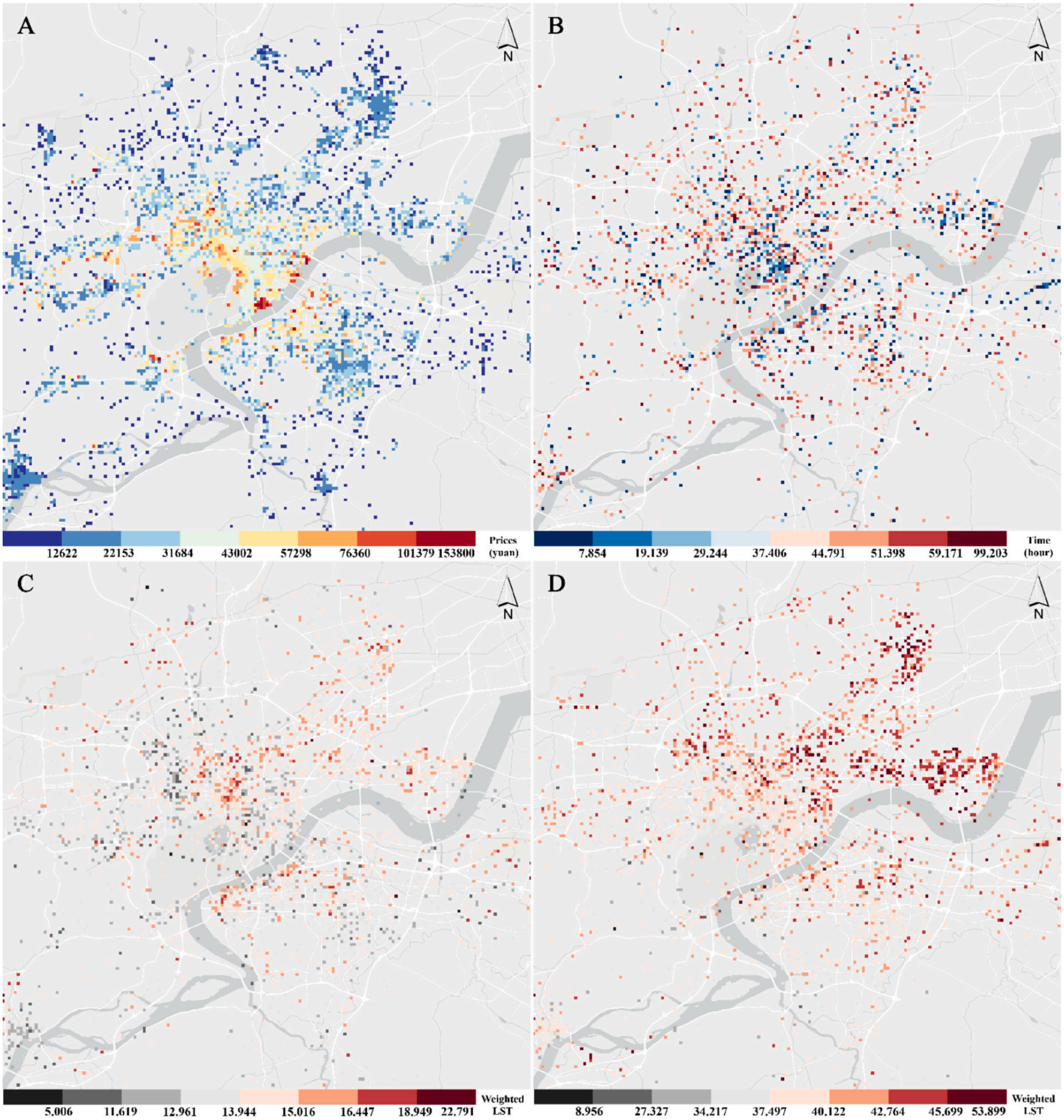

Fig. 6. Spatial distribution of key variables across the Hangzhou study area. (A) Average housing prices (yuan/m^2), (B) Total mobility-based exposure duration (hours), (C) Average summer MBE, and (D) Average winter MBE.

$$S = p_i \mid t_i \in [00:00, 06:00] \wedge d_i \geq 120$$

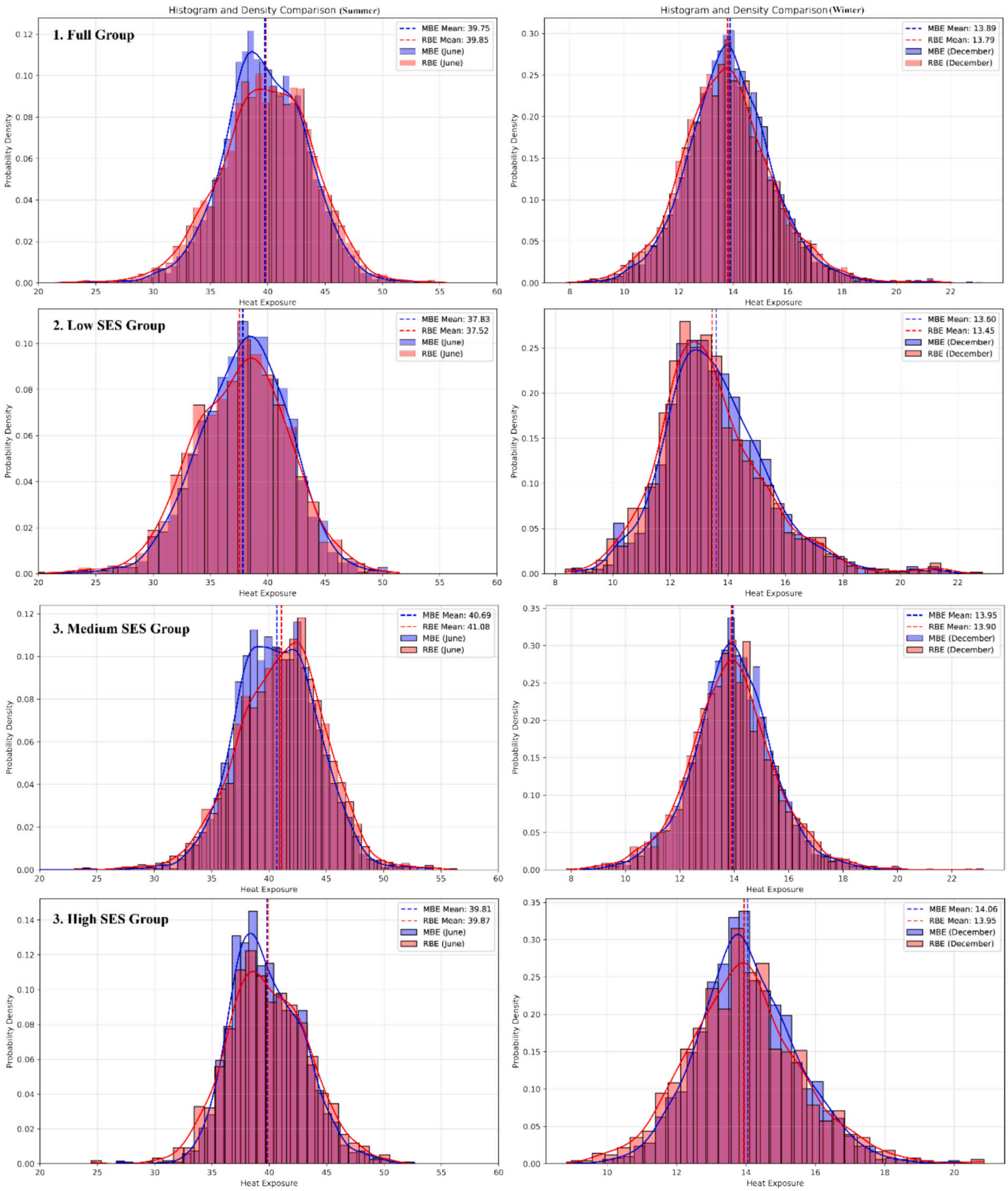

Fig. 7. Histogram and density distribution comparison between MBE and RBE across different socioeconomic status groups during summer (June) and winter (December). The distributions are shown for full samples (top row), low SES samples (second row), medium SES samples (third row), and high SES samples (bottom row). Blue histograms and dashed lines represent MBE distributions, while red histograms and solid lines represent RBE distributions. Vertical dashed lines indicate the mean values. Heat exposure values are measured in degrees Celsius. (For interpretation of the references to colour in this figure legend, the reader is referred to the web version of this article.)

where S is the set of valid stay points, p_i represents a location point with coordinates $\left(x_i, y_i\right)$, t_i is the timestamp, and d_i is the duration in minutes. Next, we implement a time-weighting scheme where each stay point is weighted by its duration. For each point p_i with duration d_i, we generate a set of weighted points:

$$W_i = w_{ij} \mid w_{ij} = (x_i, y_i), j = 1, 2, \ldots, \lfloor d_i \rfloor$$

The complete weighted point set W is the union of all individual weighted point sets:

$$W = \cup_{i=1}^{n} W_i$$

Finally, we apply K-means clustering (k = 1) to identify the home location. The algorithm minimizes the within-cluster sum of squared distances:

$$\underset{\mu}{\mathrm{argmin}} \sum_{w \in W} |w - \mu|^2$$

where μ represents the cluster centroid. The algorithm is run for multiple iterations with different initial conditions, and the solution with the lowest objective function value is selected:

$$home_{location} = \underset{t=1}{\overset{500}{\mathrm{argmin}}} \sum_{w \in W} |w - \mu_t|^2$$

where μ_t is the centroid from the t-th iteration. The final centroid coordinates represent the estimated residential location of the resident. This approach effectively leverages temporal patterns in human mobility by employing a time-weighting scheme that ensures locations with longer stay durations exert greater influence on the result. The multiple iteration strategy helps avoid local optima and enhances identification reliability. The generated residential location accounts for the collective influence of multiple cell towers, making the centroid-based approach more accurate in identifying the person's residences compared to simply selecting the cell tower with the longest stay duration. Similar methodologies have been extensively applied in studies focusing on residential area identification (Sun et al., 2021).

4. Results

Before quantitatively examining the NEAP, we first visualized the spatial distribution of key variables across the study area, as shown in Fig. 6. Fig. 6A shows the spatial distribution of housing prices across Hangzhou. Higher prices (shown in warmer colors) are concentrated in the central urban areas, while lower prices (cooler colors) are observed in peripheral regions. Fig. 6B displays the total exposure duration of residents included in the analysis, with durations varying from 7 to 99.203 h. Fig. 6C and D illustrate the average mobility-based heat exposure (MBE) of summer and winter respectively, revealing distinct spatial patterns of thermal exposure across the urban landscape. These distributions provide the database for the subsequent NEAP analysis.

4.1. The NEAP results

Due to more cloudy and rainy weather in summer resulting in higher LST coverage gaps, we selected mobility trajectories of 5747 residents for summer analysis. In winter, with fewer cloudy days, we selected 6167 residents for the study. Overall, the summer MBE average was 39.75 °C while RBE was 39.85 °C. The winter MBE average was 13.89 °C while RBE was 13.79 °C. Using RBE as a baseline,

Table 1
Comparison of Four NEAP Test Results Across Different Socioeconomic Status Groups.

Group	Summer Overall	Low SES	Medium SES	High SES	Winter Overall	Low SES	Medium SES	High SES
Sample Size	5747	1547	2881	1319	6167	1639	3134	1394
NEAP Strength	*(4/4)*	*(4/4)*	*(3/4)*	*(3/4)*	*(3/4)*	*(3/4)*	*(3/4)*	*(3/4)*
t-Statistic	−4.28	−4.44	0.2	−3.26	−6.75	−6.84	−2.28	−3.76
p-Value	*<0.01*	*<0.01*	*0.837*	*0.01*	*<0.01*	*<0.01*	*<0.05*	*<0.01*
RBE Standard Deviation	*4.31*	*4.77*	*3.82*	*3.55*	*1.72*	*1.91*	*1.61*	*1.66*
MBE Standard Deviation	4	4.63	3.5	3.17	1.59	1.83	1.48	1.46
SD Reduction %	*7.02*	*2.97*	*8.41*	*10.59*	*7.51*	*3.95*	*7.84*	*11.91*
IQR Reduction %	7.58	7.93	5.29	6.17	7.35	−1.44	8.11	10.93
RBE Near-Mean %	*39.64*	*42.02*	*38.25*	*37.38*	*42.68*	*42.34*	*42.53*	*41.82*
MBE Near-Mean %	40.28	44.6	38.63	34.95	41.9	40.51	42.15	41.03
Near-Mean Increase	*0.64*	*2.59*	*0.38*	*−2.43*	*−0.78*	*−1.83*	*−0.38*	*−0.79*
Q1%	19.71	21.78	18.26	18.95	18.14	17.45	17.55	17.14
Q2%	*32.71*	*34*	*31.73*	*34.87*	*35.43*	*37.89*	*35.23*	*36.15*
Q3%	15.75	12.61	16.35	16.53	16.07	18.61	15.32	15.42
Q4%	*31.27*	*31.16*	*33.11*	*28.96*	*29.72*	*25.75*	*31.27*	*30.27*
NEAP Evidence %	63.98	65.16	64.84	63.84	65.15	63.64	66.5	66.43

Note: Near-mean samples are defined as samples falling within the range of mean ± 0.5 standard deviation.

this indicates that human mobility behavior tends to reduce heat exposure levels in summer while increasing them in winter. This finding suggests that human activities tend to "improve" residents' exposure conditions, with directionally different effects across seasons.

Furthermore, based on housing price data shown in Fig. 6, we matched housing prices to identified residential addresses to classify residents' socioeconomic status (Nilforoshan et al., 2023). Residents were categorized as high SES (top 25%), low SES (bottom 25%), and medium SES (remaining 50%). Using this grouping method, we calculated heat exposure density distribution curves for six resident groups across summer and winter (Fig. 7, the density curves demonstrate the variations in exposure patterns across different SES groups and seasons, revealing distinct NEAP effects among different socioeconomic groups) and validated the NEAP effect using the four previously mentioned methods (Table 1).

In the full sample NEAP tests, the individual-based pairwise differences between RBE and MBE were statistically significant ($p < 0.01$) across both seasons. The standard deviation decreased from 4.31 (RBE) to 4.00 (MBE) for summer samples and from 1.72 (RBE) to 1.50 (MBE) for winter samples. This indicates greater variation in summer heat exposure (SD $>$ 4) compared to winter (SD $<$ 2). Moreover, after considering human mobility, the proportion of near-mean samples increased from 39.64% to 40.28% in summer and decreased from 42.68% to 41.90% in winter, showing modest overall changes. In the scatter plot and quadrant analysis, the proportion of NEAP evidence (both upward and downward averaging) exceeded 60%, demonstrating a strong NEAP effect.

As shown in Table 1, in summer heat exposure calculations, the NEAP effect was more pronounced among low SES residents. Compared to the full sample, they showed higher proportions in Q1 and Q2 (high exposure increase and low exposure increase, accounting for 21.78% and 34% of low SES resident samples, respectively). In contrast, high SES residents showed higher proportions in Q3 (16.53%, low exposure decrease) and Q4 (28.96%, high exposure decrease) compared to low SES residents (12.61% and 31.16%,

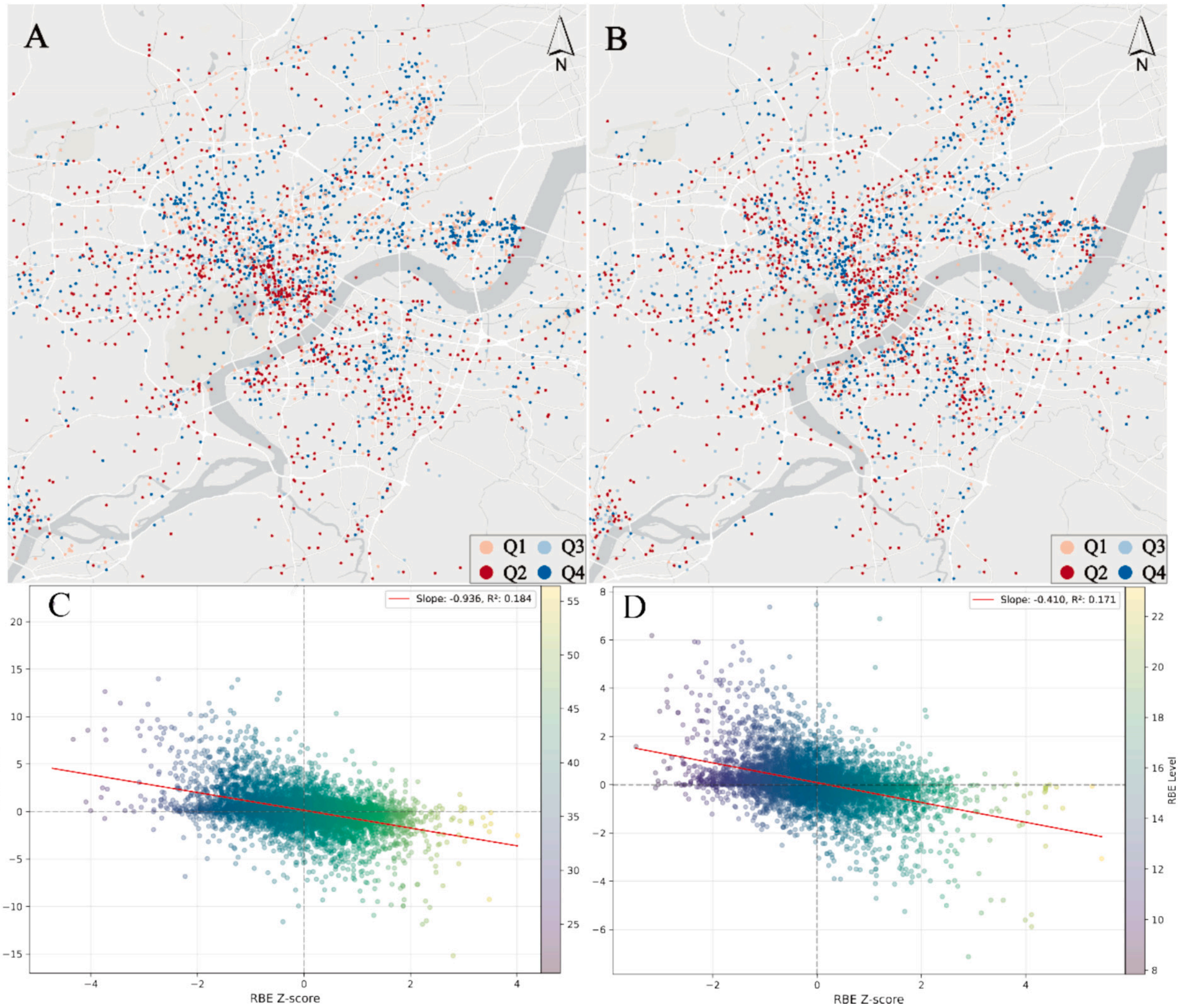

Fig. 8. Spatial Distribution and scatter plot of NEAP Types (Q1-Q4) in Summer (left) and Winter (right) Seasons. The figure illustrates the geographical clustering patterns of different mobility-based exposure adjustments, where Q1 represents increased high exposure, Q2 represents increased low exposure, Q3 represents decreased low exposure, and Q4 represents decreased high exposure.

respectively). This indicates that high SES groups typically face less extreme heat wave impacts in summer, while low SES residents often encounter higher heat exposure risks after considering human mobility. However, this disparity was not as evident during the winter season.

4.2. The spatial distribution patterns of different NEAP patterns

As shown in Table 1, we assigned each resident to one of the Q1-Q4 categories (including averaging and polarization), representing high exposure value increase, low exposure value increase, low exposure value decrease, and high exposure value decrease, respectively. The distribution of the NEAP test results show consistent patterns across seasons to some extent, with Q2 (low RBE value increase) being the dominant pattern (summer: 32.71%, winter: 35.43%), followed by Q4 (high RBE value decrease) (summer: 31.27%, winter: 29.72%). This indicates that human mobility behavior systematically moderates extreme exposure levels, although the spatial patterns vary across seasons. We mapped the geographical distribution of Q1-Q4 based on residents' residential addresses, as shown in Fig. 8.

An intuitive conclusion is that main urban areas exhibit a stronger "upward averaging effect" (Q2), while newly developed urban areas tend to show a "downward averaging effect" (Q4), which is consistent with those of Wu et al. (2025). This may be due to the higher proportion of impervious surfaces, incomplete municipal greening, and significant industrial activities in newly developed areas, which can result in higher residential heat exposure. People living in the newly developed areas moving to the cooler workplace could reduce their individual overall heat exposure level. In contrast, residents living in the main urban area will enjoy a lower heat RBE and a relatively higher heat MBE.

To analyze the spatial distribution characteristics of different neighborhood effect averaging patterns, we calculated global Moran's I values as shown in Table 2 (assigning values 1, 2, 3, 4 to residents, representing different NEAP types). The summer Moran's I value was 0.030, while the winter value was 0.036. These results indicate weak but statistically significant spatial autocorrelation ($p < 0.001$). The spatial dispersion analysis reveals distinct seasonal characteristics, with winter showing slightly stronger spatial clustering (z-score: 6.237) compared to summer (z-score: 5.118). Specifically, among the different NEAP patterns, Q2 exhibits the highest spatial dispersion (0.289) in summer. Given that the mobility data was held constant, this dispersion is not due to behavioral changes but likely reflects the interaction between the fixed travel patterns and the heterogeneous summer LST distribution. In contrast, Q1 displays the highest dispersion (0.328) in winter. This suggests that when the same mobility patterns are applied to the winter LST map, the resulting exposure changes for those with high RBE become more spatially dispersed, likely driven by the unique spatial characteristics of the winter thermal environment.

5. Discussion and conclusion

In this study, by analyzing the differences between MBE and RBE, we demonstrated that the NEAP effect is prevalent in urban heat exposure and significant across different SES groups. We found that approximately 65% of residents exhibited neighborhood effect averaging (including low-value increases and high-value decreases), strongly supporting the self-regulation of extreme environmental exposure through human mobility patterns. This finding holds particular significance in the context of intensifying urban heat island effects and climate change.

Our findings share commonalities with previous studies on air pollution exposure (Kim and Kwan, 2021b) and green space exposure (Zheng et al., 2024), where people's daily activity patterns tend to average out their environmental exposures. They also support the notion of regression to the mean in people's MBE as suggested by Cai and Kwan (2024). However, our study uniquely discovered seasonal variations in NEAP effects: with low SES groups showing stronger heat exposure NEAP effects in summer, while high SES groups exhibited more pronounced effects in winter.

Compared to previous human mobility studies primarily based on individual-level survey methods, this research introduced spatio-temporal big data represented by mobile phone signaling data and remote sensing imagery, addressing the limitations of traditional survey methods such as high costs and limited coverage. While maintaining privacy protection, our study overcame constraints faced by similar spatio-temporal big data research, such as difficulties in identifying residential addresses and obtaining individual attributes. First, by combining mobile phone signaling big data with trajectory clustering algorithms, we more accurately identified residents' home addresses, providing a more reliable spatial information for environmental exposure assessment. Second, through the integration of real estate data, we could better understand and quantify thermal exposure differences among different SES groups. This approach achieved broad coverage while obtaining necessary individual attribute statistics.

Table 2
Global Spatial Autocorrelation and Dispersion Metrics of the NEAP Across Seasons.

Group	Summer Overall	Summer	Winter
Spatial Autocorrelation	Global Moran's I	0.03	0.036
	p-value	0.001	0.001
	z-score	5.118	6.237
Spatial Dispersion	Q1	0.187	0.328
	Q2	0.289	0.228
	Q3	0.281	0.2
	Q4	0.217	0.304

Our results revealed significantly different exposure patterns across socioeconomic groups, particularly in seasonal variations. During summer, low SES residents experienced more pronounced NEAP effects (may have some activity likes: construction, delivery services, street vending), while in winter, high SES residents experienced more NEAP effects (may flexibility in timing and location choices for both work and leisure activities). The scatter plot analysis indicated that low SES residents often face higher risks of heat exposure. To improve this situation, it is necessary to reduce the heat exposure in both their residential and workplace environments. For instance, priority should be placed on planting trees and developing parks and green infrastructure in communities predominantly inhabited by low-SES residents. Furthermore, enhancing heat protection measures in workplaces is also crucial to reduce their overall heat exposure.

However, this study also has several limitations. The spatiotemporal big data approach may not fully reflect residents' actual exposure levels, as individuals might reduce their thermal exposure through means such as air conditioning or sun-protective clothing. Additionally, while our study covered 16,186 base stations, our method's spatial accuracy is slightly inferior to traditional citizen science approaches that record precise GPS locations. Future research could address these issues by incorporating individual behavioral survey data to better understand population exposure regulation behaviors and decision-making mechanisms. It is important to note that LST represents the outdoor surface temperature. As the mobile phone data does not distinguish between indoor and outdoor locations, our calculation of "heat exposure" refers to the ambient outdoor LST at a person's location, which serves as a proxy for potential exposure. This approach does not account for micro-environments or protective behaviors (e.g., being inside an air-conditioned building), a limitation discussed further in the Discussion section.

Funding Acknowledgments

This research was supported by grants from the Hong Kong Research Grants Council (General Research Fund Grant no. 14605920, 14606922, 14603724; Collaborative Research Fund Grant no. C4023-20GF; Research Matching Grants RMG 8601219, 8601242, 3110151), a grant from the Research Committee on Research Sustainability of Major Research Grants Council Funding Schemes (3133235) of the Chinese University of Hong Kong (CUHK), a grant from the 1+1+1 CUHK-CUHK(SZ)-GDSTC Joint Collaboration Fund (4760974, 2025A0505000062), a grant from the Vice-Chancellor's One-off Discretionary Fund (Smart and Sustainable Cities: City of Commons) (4930787) of CUHK, Open Fund of State Key Laboratory of Information Engineering in Surveying, Mapping and Remote Sensing, Wuhan University, and the National Natural Science Foundation of China (42501579). The funders had no role in the study design, data collection, data analysis, decision to publish, or preparation of the manuscript. The authors declare that they have no financial and personal relationships with other people or organizations that can inappropriately influence our work.

CRediT authorship contribution statement

Yan Zhang: Writing – original draft, Visualization, Methodology, Conceptualization. **Mei-Po Kwan:** Writing – review & editing, Resources, Project administration, Investigation, Funding acquisition, Conceptualization. **Zhijie Zhang:** Formal analysis, Data curation.

Declaration of competing interest

The authors declare that they have no known competing financial interests or personal relationships that could have appeared to influence the work reported in this paper. The research funding received from various organizations including the Hong Kong Research Grants Council and The Chinese University of Hong Kong had no role in study design, data collection and analysis, decision to publish, or preparation of the manuscript."

Data availability

Data will be made available on request.

References

Cai, J., Kwan, M.P., 2024. The universal neighborhood effect averaging in mobility-dependent environmental exposures. Environ. Sci. Technol. 58 (45), 20030–20039.

Chen, B., Wu, S., Song, Y., et al., 2022. Contrasting inequality in human exposure to greenspace between cities of global north and global south. Nat. Commun. 13 (1), 4636.

Chen, Z., Zou, T., Xu, Z., et al., 2024. SAGE-GSAN: a graph-based method for estimating urban taxi CO emissions using street view images. J. Clean. Prod. 474, 143543.

Falchetta, G., De Cian, E., Sue Wing, I., et al., 2024. Global projections of heat exposure of older adults. Nat. Commun. 15 (1), 3678.

Garber, M.D., Teyton, A., Jankowska, M.M., et al., 2024. Is home where the heat is? Comparing residence-based with mobility-based measures of heat exposure in San Diego, California. J. Expo. Sci. Environ. Epidemiol. 1–11.

Hu, T., Wang, S., She, B., et al., 2021. Human mobility data in the COVID-19 pandemic: characteristics, applications, and challenges. Int. J. Digital Earth 14 (9), 1126–1147.

Huang, J., Kwan, M.P., 2022. Uncertainties in the assessment of COVID-19 risk: a study of people's exposure to high-risk environments using individual-level activity data. Ann. Am. Assoc. Geogr. 112 (4), 968–987.

Huang, X., Jiang, Y., Mostafavi, A., 2024. The emergence of urban heat traps and human mobility in 20 US cities. npj Urban Sustain. 4 (1), 6.

Kim, J., Kwan, M.P., 2021a. How neighborhood effect averaging might affect assessment of individual exposures to air pollution: a study of ozone exposures in Los Angeles. Ann. Am. Assoc. Geogr. 111 (1), 121–140.
Kim, J., Kwan, M.P., 2021b. Assessment of sociodemographic disparities in environmental exposure might be erroneous due to neighborhood effect averaging: implications for environmental inequality research. Environ. Res. 195, 110519.
Kumakura, E., Ashie, Y., Ueno, T., 2024. Assessing the impact of summer heat on the movement of people in Tokyo based on mobile phone location data. Build. Environ. 265, 111952.
Kwan, M.P., 2016. Algorithmic geographies: big data, algorithmic uncertainty, and the production of geographic knowledge. Ann. Am. Assoc. Geogr. 106 (2), 274–282.
Kwan, M.P., 2018. The neighborhood effect averaging problem (NEAP): an elusive confounder of the neighborhood effect. Int. J. Environ. Res. Public Health 15 (9), 1841.
Li, J., Liu, H., Chen, X., et al., 2021. Predicting and Understanding Human Mobility Based on Social Media Check-in Data[C]//Spatial Data and Intelligence: Second International Conference, SpatialDI 2021. Springer International Publishing, Hangzhou, China, pp. 148–163. April 22–24, 2021, proceedings 2.
Liu, Z., Liu, C., Mostafavi, A., 2023. Beyond residence: a mobility-based approach for improved evaluation of human exposure to environmental hazards. Environ. Sci. Technol. 57 (41), 15511–15522.
Liu, D., Zhou, R., Ma, Q., et al., 2024. Spatio-temporal patterns and population exposure risks of urban heat island in megacity Shanghai, China. Sustain. Cities Soc. 108, 105500.
Liu, Y., Kwan, M.P., Wang, J., 2025a. Analytically articulating the effect of buffer size on urban green space exposure measures. Int. J. Geogr. Inf. Sci. 39 (2), 255–276.
Liu, Y., Kwan, M.P., Song, L., Yu, C., Cui, Y., 2025b. How mobility-based exposure measures may mitigate the underestimation of the association between green space exposures and health. Soc. Sci. Med. 379, 118190.
Ma, L., Huang, G., Johnson, B.A., et al., 2023. Investigating urban heat-related health risks based on local climate zones: a case study of Changzhou in China. Sustain. Cities Soc. 91, 104402.
Malekzadeh, M., Reuschke, D., Long, J.A., 2024. Quantifying local mobility patterns in urban human mobility data. Int. J. Geogr. Inf. Sci. 1–24.
Münzel, T., Sørensen, M., Hahad, O., et al., 2023. The contribution of the exposome to the burden of cardiovascular disease. Nat. Rev. Cardiol. 20 (10), 651–669.
Nilforoshan, H., Looi, W., Pierson, E., et al., 2023. Human mobility networks reveal increased segregation in large cities. Nature 624 (7992), 586–592.
Sabedotti, M.E.S., O'Regan, A.C., Nyhan, M.M., 2023. Data insights for sustainable cities: associations between Google street view-derived urban greenspace and Google air view-derived pollution levels. Environ. Sci. Technol. 57 (48), 19637–19648.
Schläpfer, M., Dong, L., O'Keeffe, K., et al., 2021. The universal visitation law of human mobility. Nature 593 (7860), 522–527.
Song, J., Zhou, S., Kwan, M.P., et al., 2025. Association between real-time noise exposure in broader activity contexts and job satisfaction: evidence from Guangzhou, China. Cities 161, 105912.
Sun, H., Chen, Y., Lai, J., et al., 2021. Identifying tourists and locals by K-means clustering method from mobile phone signaling data. J. Transp. Eng. Part A Syst. 147 (10), 04021070.
Wang, Q., Phillips, N.E., Small, M.L., et al., 2018. Urban mobility and neighborhood isolation in America's 50 largest cities. Proc. Natl. Acad. Sci. 115 (30), 7735–7740.
Wang, C., Ren, Z., Guo, Y., et al., 2024a. Assessing urban population exposure risk to extreme heat: patterns, trends, and implications for climate resilience in China (2000−2020). Sustain. Cities Soc. 103, 105260.
Wang, J., Kwan, M.P., Xiu, G., et al., 2024b. Investigating the neighborhood effect averaging problem (NEAP) in greenspace exposure: a study in Beijing. Landsc. Urban Plan. 243, 104970.
Wang, L., Zhou, S., Zheng, Z., et al., 2025a. Unveiling the neighborhood effect averaging problem: the role of daily mobility in shaping built-environment quality exposure. Ann. Am. Assoc. Geogr. 115 (2), 264–281.
Wang, J., Liu, Y., Kwan, M.P., 2025b. Cross-validation between GPS-derived trajectories and activity-travel diaries for transport geography studies. J. Transp. Geogr. 126, 104239.
Wei, J., Li, Z., Lyapustin, A., et al., 2021. Reconstructing 1-km-resolution high-quality PM2. 5 data records from 2000 to 2018 in China: spatiotemporal variations and policy implications. Remote Sens. Environ. 252, 112136.
Wei, L., Donaire-Gonzalez, D., Helbich, M., et al., 2024. Validity of mobility-based exposure assessment of air pollution: a comparative analysis with home-based exposure assessment. Environ. Sci. Technol. 58 (24), 10685–10695.
Wei, L., Helbich, M., Flückiger, B., et al., 2025. Variability in mobility-based air pollution exposure assessment: effects of GPS tracking duration and temporal resolution of air pollution maps. Environ. Int. 198, 109454. https://doi.org/10.1016/j.envint.2025.109454. ISSN 0160-4120.
Wu, H., Zhang, G., Liu, Y., et al., 2025. Addressing neighborhood effect averaging problem: distinguishing mobility-based and residence-based heat exposure. Build. Environ. 280, 113139. https://doi.org/10.1016/j.buildenv.2025.113139. ISSN 0360-1323.
Yasumoto, S., Jones, A.P., Oyoshi, K., et al., 2019. Heat exposure assessment based on individual daily mobility patterns in Dhaka, Bangladesh. Comput. Environ. Urban. Syst. 77, 101367.
Yin, Y., Grundstein, A., Mishra, D.R., et al., 2021. DTEx: a dynamic urban thermal exposure index based on human mobility patterns. Environ. Int. 155, 106573.
Yuan, B., Zhou, L., Hu, F., et al., 2022. Diurnal dynamics of heat exposure in Xi'an: a perspective from local climate zone. Build. Environ. 222, 109400.
Zhang, Y., Kwan, M.P., 2025. Considering human mobility is essential for accurate environmental exposure assessment. Sci. Bull. 70 (21), 3457–3460. https://doi.org/10.1016/j.scib.2025.07.016. ISSN 2095-9273.
Zhang, J., Yao, X., Chen, Y., et al., 2024a. Spatiotemporal dynamic mapping of heat exposure risk for different populations in city based on hourly multi-source data. Sustain. Cities Soc. 107, 105454.
Zhang, Y., Kwan, M.P., Ma, H., 2024b. Sensing noise exposure and its inequality based on noise complaint data through vision-language hybrid method. Appl. Geogr. 171, 103369.
Zhang, Y., Kwan, M.P., Ma, H., et al., 2026. Social media big data reveals how mobility reshapes human environmental exposure inequality. Landsc. Urban Plan. 270, 105600. https://doi.org/10.1016/j.landurbplan.2026.105600.
Zhang, Y., Kwan, M.P., Yu, B., et al., 2025. Quantitative identification of mixed urban functions: a probabilistic approach based on physical and social sensing data. Trans. GIS 29 (1), e13272.
Zheng, L., Kwan, M.P., Liu, Y., et al., 2024. How mobility pattern shapes the association between static green space and dynamic green space exposure. Environ. Res. 258, 119499.